

Experimental observation of pseudogap in a modulation-doped Mott insulator: Sn/Si(111)-($\sqrt{3}\times \sqrt{3}$)*R*30°

Yan-Ling Xiong(熊艳翎), Jia-Qi Guan(关佳其), Rui-Feng Wang(汪瑞峰), Can-Li Song(宋灿立), Xu-Cun Ma(马旭村), and Qi-Kun Xue(薛其坤)

Citation: Chin. Phys. B, 2022, 31 (**6**): 067401. DOI: 10.1088/1674-1056/ac65f2
Journal homepage: http://cpb.iphy.ac.cn; http://iopscience.iop.org/cpb

What follows is a list of articles you may be interested in

Fabrication and characterization of Al-Mn superconducting films for applications in TES bolometers

Qing Yu(余晴), Yi-Fei Zhang(张翼飞), Chang-Hao Zhao(赵昌昊), Kai-Yong He(何楷泳), Ru-Tian Huang(黄汝田), Yong-Cheng He(何永成), Xin-Yu Wu(吴歆宇), Jian-She Liu(刘建设), and Wei Chen(陈炜)

Chin. Phys. B, 2021, 30 (**7**): 077402. DOI: 10.1088/1674-1056/abe0c6

NBN-doped nanographene embedded with five- and seven-membered rings on Au(111) surface

Huan Yang(杨欢), Yun Cao(曹云), Yixuan Gao(高艺璇), Yubin Fu(付钰彬), Li Huang(黄立), Junzhi Liu(刘俊治), Xinliang Feng(冯新亮), Shixuan Du(杜世萱), and Hong-Jun Gao(高鸿钧)

Chin. Phys. B, 2021, 30 (**5**): 056802. DOI: 10.1088/1674-1056/abeede

Superconductivity in twisted multilayer graphene: A smoking gun in recent condensed matter physics

Yonghuan Chu(楚永唤), Fangduo Zhu(朱方铎), Lingzhi Wen(温凌志), Wanying Chen(陈婉莹), Qiaoni Chen(陈巧妮), and Tianxing Ma(马天星)

Chin. Phys. B, 2020, 29 (**11**): 117401. DOI: 10.1088/1674-1056/abbbea

Unconventional chiral d-wave superconducting state in strained graphene

Feng Xu(徐峰), Lei Zhang(张磊)

Chin. Phys. B, 2019, 28 (**11**): 117403. DOI: 10.1088/1674-1056/ab478c

Tunable superconductivity in parent cuprate $Pr_2CuO_{4\pm\delta}$ thin films

Xinjian Wei(魏鑫健), Ge He(何格), Wei Hu(胡卫), Xu Zhang(张旭), Mingyang Qin(秦明阳), Jie Yuan(袁洁), Beiyi Zhu(朱北沂), Yuan Lin(林媛), Kui Jin(金魁)

Chin. Phys. B, 2019, 28 (**5**): 057401. DOI: 10.1088/1674-1056/28/5/057401

RAPID COMMUNICATION

Experimental observation of pseudogap in a modulation-doped Mott insulator: Sn/Si(111)-($\sqrt{3}\times\sqrt{3}$)$R30^\circ$

Yan-Ling Xiong(熊艳翎)[1], Jia-Qi Guan(关佳其)[1], Rui-Feng Wang(汪瑞峰)[1], Can-Li Song(宋灿立)[1,2,†], Xu-Cun Ma(马旭村)[1,2,‡], and Qi-Kun Xue(薛其坤)[1,2,3,4]

[1] *State Key Laboratory of Low-Dimensional Quantum Physics, Department of Physics, Tsinghua University, Beijing* 100084, *China*
[2] *Frontier Science Center for Quantum Information, Beijing* 100084, *China*
[3] *Beijing Academy of Quantum Information Sciences, Beijing* 100193, *China*
[4] *Southern University of Science and Technology, Shenzhen* 518055, *China*

(Received 1 March 2022; revised manuscript received 28 March 2022; accepted manuscript online 11 April 2022)

Unusual quantum phenomena usually emerge upon doping Mott insulators. Using a molecular beam epitaxy system integrated with cryogenic scanning tunneling microscope, we investigate the electronic structure of a modulation-doped Mott insulator Sn/Si(111)-($\sqrt{3}\times\sqrt{3}$)$R30^\circ$. In underdoped regions, we observe a universal pseudogap opening around the Fermi level, which changes little with the applied magnetic field and the occurrence of Sn vacancies. The pseudogap gets smeared out at elevated temperatures and alters in size with the spatial confinement of the Mott insulating phase. Our findings, along with the previously observed superconductivity at a higher doping level, are highly reminiscent of the electronic phase diagram in the doped copper oxide compounds.

Keywords: pseudogap (PG), modulation doping, Mott insulator, scanning tunneling microscope (STM)

PACS: 74.72.Kf, 81.15.−z, 68.37.Ef, 68.37.−d **DOI:** 10.1088/1674-1056/ac65f2

1. Introduction

Mott insulators are materials in which constituent electrons cannot move freely because of strong electron repulsions and lie at the heart of strongly correlated electron physics. Upon chemical doping, the electrons delocalize and the Mott insulators can become conductive and even superconductive via a process well-known as Mott transition.[1–3] Following this transition, many unusual phenomena emerge and have been largely explored in one archetypal example of the perovskite-type copper oxide compounds. These include, for example, the unconventional superconductivity with a record critical temperature (T_c) at ambient atmosphere,[4] the pseudogap (PG) phase above T_c[5] and various different symmetry-broken states.[5–7] Among these phenomena, the PG phase stands out and continues to attract attention, because clarifying its microscopic origin from either the preformed Cooper pairs[8–10] or some competing orders[11–13] has been considered as an essential prerequisite to understanding the high-T_c superconductivity in cuprates. After more than three decades of study, however, the PG phenomenology, which turns out to be more prominent in underdoped regions, remains one of the greatest mysteries in the high-T_c cuprate superconductors.

Adsorption of metal atoms (such as Pb, In, and Tl) on semiconductor substrates (e.g., Si(111)) often induces rich surface superstructures and intriguing electronic states at the two-dimensional (2D) limit, including superconductivity,[14–17] charge density waves[18,19] and unusual magnetism.[20] Specifically, adsorption of one-third monolayer (ML) Sn on Ge(111) and Si(111) leads to the formation of a ($\sqrt{3}\times\sqrt{3}$)$R30^\circ$ reconstruction known as α phase.[21–23] Such a triangular lattice, which is characteristic of half-filled dangling bond orbitals, forms a conceptually simple and alternative system to explore correlation related Mott physics in the 2D situation.[24–26] Intriguingly, a superconducting state of $T_c \sim 4.7$ K has been recently observed in Sn/Si(111)-($\sqrt{3}\times\sqrt{3}$)$R30^\circ$ (hereinafter referred to as $\sqrt{3}$-Sn) on chemical doping by employing heavily boron-doped Si substrates.[27] Such a charge transfer mechanism has been well known as modulation doping in semiconductor heterostructures[28–30] and recently evidenced in cuprates,[31,32] thereby calling for further investigation of possible commonalities and distinctions between the doped $\sqrt{3}$-Sn and cuprates.

To date, however, only limited experiments were performed, especially leaving the electronic structure of $\sqrt{3}$-Sn in underdoped regions poorly understood. It remains a puzzle whether the opened energy gap at the Fermi level (E_F) from the tunneling experiment[33] relates to superconductivity, and if no why the Coulomb gap increases in magnitude with increasing doping concentration. Here we resolve this issue by combining a molecular beam epitaxy system (MBE) with cryogenic scanning tunneling microscope (STM). We reveal the PG nature for the opened gap in the underdoped regions, which in-

†Corresponding author. E-mail: clsong07@mail.tsinghua.edu.cn
‡Corresponding author. E-mail: xucunma@mail.tsinghua.edu.cn

© 2022 Chinese Physical Society and IOP Publishing Ltd

stead decreases with increasing doping. These behaviors bear a close resemblance to the established electronic phase diagram in cuprate superconductors.

2. Experiment

All experiments were carried out in a commercial ultrahigh vacuum (UHV) STM apparatus (Unisoku USM 1300), integrated with an MBE chamber for *in-situ* sample preparation. A magnetic field up to 11 T can be applied perpendicular to the sample surface. The base pressure for both chambers is better than 2.5×10^{-10} Torr. Two distinct p-type Si(111) wafers (boron-doped) with room temperature resistivities of 0.01 Ω·cm and 0.001 Ω·cm, respectively, were used as substrates for the $\sqrt{3}$-Sn growth. Clean Si(111)-7×7 surfaces were obtained by repeatedly flashing well-degassed substrates at 1200 °C. The $\sqrt{3}$-Sn phase was then prepared by evaporating high-purity (99.9999%) Sn from a standard Knudsen cell on Si(111) at approximately 550 °C. All STM measurements were conducted at 4.2 K using sharp polycrystalline PtIr tips, which were routinely cleaned by electron beam bombardment in MBE and appropriately calibrated on MBE-prepared Ag/Si(111) films. The STM topographies were acquired in a constant-current mode with the bias V applied to the sample, while the tunneling spectra were measured using a standard lock-in technique with a small bias modulation at 919 Hz.

3. Results and discussion

Figure 1(a) shows a representative STM topography of $\sqrt{3}$-Sn prepared on the 0.001 Ω·cm Si substrates, with the bright spots denoting the Sn adatoms. They occupy the T_4 sites of the underlying Si (111) surface and are spaced ∼ 6.6 Å apart. Individual Sn vacancies occur as dark contrast that change little with the sample bias. Figure 1(b) plots a series of differential conductance $\mathrm{d}I/\mathrm{d}V$ spectra (from bottom to top) taken along a trajectory (marked by the black arrow) approaching a single Sn vacancy in Fig. 1(a). As anticipated, the Mott–Hubbard bands could be readily identified spectroscopically. In line with a previous report,[34] every $\mathrm{d}I/\mathrm{d}V$ spectrum can be nicely decomposed into six Gaussian peaks (see the best fit of the bottom one to multiple Gaussian function), derived from the slightly appearing valence band (VB), lower Hubbard band (LHB), quasiparticle peak or saying in-gap states (IGS) at around 100 meV, and upper Hubbard band (UHB), respectively. As justified before,[34] the hole doping level of $\sqrt{3}$-Sn can be estimated by calculating the spectral weight of IGS (W_{IGS}) relative to those of UHB (W_{UHB}) and LHB (W_{LHB}) in Fig. 1(c), which was calculated by dividing W_{IGS} by the total spectral weights of W_{IGS}, W_{UHB} and W_{LHB}. Apparently, the IGS becomes less prominent in the vicinity of the Sn vacancy, indicative of a reduced hole doping level there. It is understandable because one missing Sn adatom breaks three Sn–Si bonds, leaving behind three Si dangling bonds. This contributes two extra electrons and reduces the local hole doping. Consequently, the spectral weight of UHB increases as a compensation of the significantly suppressed IGS around the Sn vacancy [Fig. 1(c)]. Such behavior resembles those of both hole- and electron-doped cuprates, in which the IGS also emerges upon doping.[32,35,36] A major difference is the occurrence of more prominent IGS in $\sqrt{3}$-Sn, which might originate from the stronger interaction between the $\sqrt{3}$-Sn and underlying Si(111) substrates.

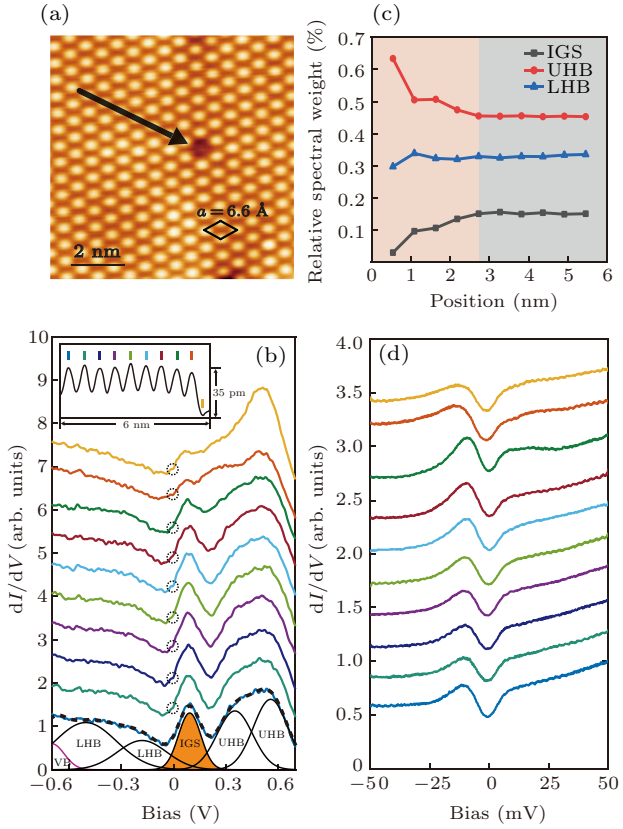


Fig. 1. (a) STM topography of $\sqrt{3}$-Sn surface (9 nm × 9 nm, $V = 200$ mV, $I = 100$ pA) with a single Sn vacancy appearing as a dark spot. (b) Large-energy-scale $\mathrm{d}I/\mathrm{d}V$ conductance spectra measured at equal separations (0.66 nm) along the black arrow in (a), color-coded to match the vertical bars (mark the positions for acquiring the $\mathrm{d}I/\mathrm{d}V$ spectra) in the inserted line profile. The bottom spectrum is illustratively fitted with multiple Gaussian peaks as denoted. Tunneling junction is stabilized at $V = 1.0$ V and $I = 150$ pA. (c) Relative spectral weights of the LHB, UHB, and IGS, calculated from their site-specific Gaussian distributions. (d) Low-energy-scale tunneling spectra ($V = 50$ mV, $I = 150$ pA) at the same positions as (b), showing a PG opening at E_{F}.

Another noteworthy feature is a small dip that universally occurs near E_{F}, circled in Fig. 1(b). To present the feature more clearly, the smaller-energy-scale $\mathrm{d}I/\mathrm{d}V$ spectra are acquired at the correspondingly identical sites and plotted in Fig. 1(d). A spatially uniform energy gap of approximately 20 meV, irrespective of the existence of Sn vacancy, is identified and symmetric with respect to E_{F}. The results are consistent with the previous findings, except that no apparent van Hove singularity is observable below E_{F} in our study.[33,34]

The robustness of the small energy gap against the Sn vacancy hints at its delocalized nature.

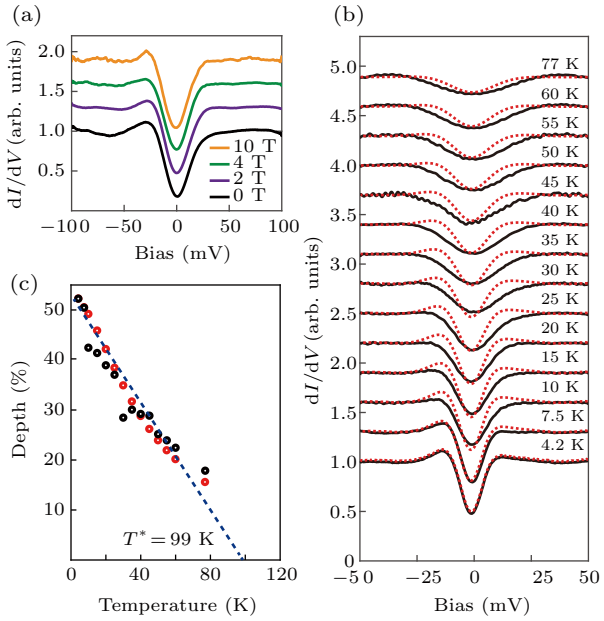


Fig. 2. (a) Tunneling conductance $\mathrm{d}I/\mathrm{d}V$ spectra ($V = 100$ mV, $I = 150$ pA) of the $\sqrt{3}$-Sn phase under various magnetic fields as indicated. (b) Variation of PG with temperature ($V = 50$ mV, $I = 150$ pA). The dotted red lines represent the thermal broadening of the spectrum at 4.2 K to the progressively increasing temperatures. (c) Plotted PG depth as a function of temperature. The black and red circles represent the values extracted from the experimental curves and the thermal broadening ones in (b), respectively, which are nicely matched to each other. The dashed line shows the best fit of PG depth to a linear function.

To provide more insights into the observed energy gap, we characterize its dependence on the external magnetic field and temperature in Fig. 2. Firstly, the gap remains essentially unchanged upon the application of a magnetic field up to 10 T [Fig. 2(a)]. This excludes its origin from a superconducting gap. Indeed, the gap magnitude of ~ 20 meV turns out to be unrealistically larger than the specific superconducting gap of ~ 1.5 meV identified in this system.[27] Figure 2(b) plots the dependence of the site-specific tunneling $\mathrm{d}I/\mathrm{d}V$ spectra on temperature ranging from 4.2 K to 77 K. At elevated temperatures, the gap gets gradually suppressed. To evaluate the temperature smearing effect, we perform the thermal broadening simulation which is a purely mathematical process. We calculate the convolution curves of the $\mathrm{d}I/\mathrm{d}V$ spectrum measured at 4.2 K with the first derivative of Fermi–Dirac function at varying temperatures and overlay them on the corresponding $\mathrm{d}I/\mathrm{d}V$ spectra by the red dashed lines. They match with each other especially for the gap depth [Fig. 2(c)], defined as the difference between unity and the normalized zero-bias conductance. This is reminiscent of the PG, which also only smears out at elevated temperatures via thermal broadening in underdoped cuprates.[6,8] By extrapolating the linear relationship of the PG depth versus temperature to the point where the gap depth is equal to zero, the transition temperature, T^*, is estimated to be around 99 K. We further compare the spectral weight of IGS relative to LHB and UHB, and therefore obtain the hole doping level of at most 8.5% for our samples investigated. This value is lower than the threshold doping level of 10% required for the emergent superconductivity.[27] This suggests that the $\sqrt{3}$-Sn samples studied here lie in the underdoped regions, which happens to match with the experimental observation of PG.

Next we explore the doping dependence of PG by taking advantage of the $\sqrt{3}$-Sn nanodomain size-dependent hole doping level, albeit unknown mechanism.[33] Here the $\sqrt{3}$-Sn nanodomains are isolated and laterally encircled by the neighboring Sn/Si(111)-$(2\sqrt{3}\times 2\sqrt{3})R30°$ (shorten as $2\sqrt{3}$-Sn) phase, as illustrated in Fig. 3(a). Figure 3(b) represents the characteristic $\mathrm{d}I/\mathrm{d}V$ spectra, disclosing well-defined PG on various $\sqrt{3}$-Sn nanodomains with varying areas. Moreover, in one specific nanodomain, we have measured a series of $\mathrm{d}I/\mathrm{d}V$ spectra at various positions, calculated the gap magnitude, and then averaged over them. More than 20 nanodomains have been measured and the results are plotted in Fig. 3(c). The PG shrinks in magnitude with increasing $\sqrt{3}$-Sn nanodomain area and saturates to about 20 meV above 600 nm^2. In extremely small $\sqrt{3}$-Sn nanodomains, a U-shaped gap develops with an apparent electron–hole asymmetry, analogous to the previous study.[33] A sharp and significant distinction is that the hole doping level, estimated from the relative spectral weight analysis just as Fig. 1(b), decreases as the area of $\sqrt{3}$-Sn nanodomains is reduced [Fig. 3(d)]. This has been unambiguously confirmed as well by exploring the spatial-dependent $\mathrm{d}I/\mathrm{d}V$ spectra perpendicular to the boundary between the $\sqrt{3}$-Sn and $2\sqrt{3}$-Sn phases in Figs. 3(e) and 3(f). Similar to those near a single Sn vacancy, the tunneling conductance $\mathrm{d}I/\mathrm{d}V$ spectra near the phase boundary are characteristic of significantly weaken IGS. This means a reduced hole doping level along the phase boundary and thus for the small $\sqrt{3}$-Sn nanodomain as a whole. The large discrepancy from the previous study might arise from either the distinct sample preparation details or the different measurement temperatures. In the previous study, the large- and small-energy scale $\mathrm{d}I/\mathrm{d}V$ spectra were separately measured at 77 K and 4.4 K, which renders a direct comparison of them probably questionable. On the other hand, we have performed all the spectroscopic $\mathrm{d}I/\mathrm{d}V$ measurements at the identical temperature of 4.2 K. This makes the present findings more convincing.

It should be noted that such PG feature has been alternatively explained as a dynamical Coulomb blockade effect.[33] Given that several different Si(111) substrates with varying doping levels have been explored and the resistive depletion layer between the $\sqrt{3}$-Sn domains and the substrates has been largely modified, the PG feature should profoundly change with the varying substrates in the Coulomb blockade model. This appears to be inconsistent from the universal occurrence of PG feature in $\sqrt{3}$-Sn, even when the underlying Si(111) substrates are more lightly doped (about 0.5%) with a resistivity of 0.01 Ω·cm [Figs. 4(a) and 4(b)]. More importantly,

if only the Coulomb blockade comes into play, the accompanying Coulomb staircase behavior commonly occurs as discrete peaks beside the Coulomb gap, which has never been observed. Thus, it seems more tempting to attribute the dip-like feature to the PG opening at E_F, as predicated from a quantum Monte Carlo simulation of the 2D Hubbard model.[37]

Figure 4(c) summarizes the doping-dependent magnitude of PG (purple stars) and the superconducting energy gap (blue star) in $\sqrt{3}$-Sn. All PG data are readily extracted from various nanodomains of $\sqrt{3}$-Sn supported by the heavily-doped Si(111) substrates (0.001 Ω·cm). It should be emphasized that we have also measured the $\sqrt{3}$-Sn on a lightly doped Si(111) substrate with the resistivity of 0.01 Ω·cm, which reveals a similar PG except for significantly suppressed gap edge peaks [Fig. 4(a)]. These behaviors resemble those of cuprate PG in a prominent manner, and the nanodomain size-dependent PG behavior is also expected for a doped 2D Mott insulator.[37]

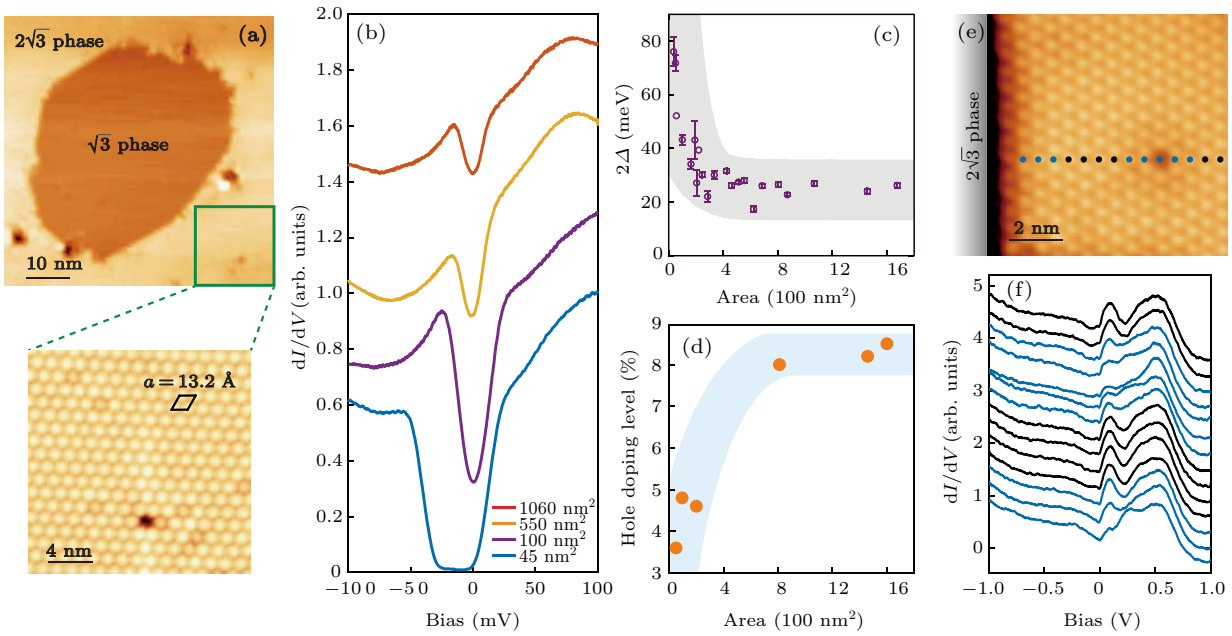


Fig. 3. (a) STM topography (60 nm × 60 nm, $V = 2.0$ V, $I = 90$ pA) showing an isolated $\sqrt{3}$-Sn domain encircled by semiconducting $2\sqrt{3}$-Sn phase. The bottom panel shows an atomically resolved STM image of the $2\sqrt{3}$-Sn surface (20 nm × 20 nm, $V = -0.7$ V, $I = 150$ pA). (b) Spatially averaged $\mathrm{d}I/\mathrm{d}V$ spectra on heterogenous $\sqrt{3}$-Sn domains with varying areas as indicated. The spectra have been vertically offset for clarity. Tunneling junction is stabilized at $V = 100$ mV and $I = 150$ pA. (c), (d) Dependence of the PG magnitude and hole doping level on the area of $\sqrt{3}$-Sn domains, respectively. The error bars in (c) denote the standard deviations of the PG magnitude on various regions of one $\sqrt{3}$-Sn domain. (e) STM topography (9 nm × 9 nm, $V = 50$ mV, $I = 100$ pA) across the boundary between the $\sqrt{3}$-Sn and $2\sqrt{3}$-Sn phases. (f) Tunneling spectra ($V = 1.0$ V, $I = 150$ pA) measured at the dot-marked sites, color-coded to match the dots in (e).

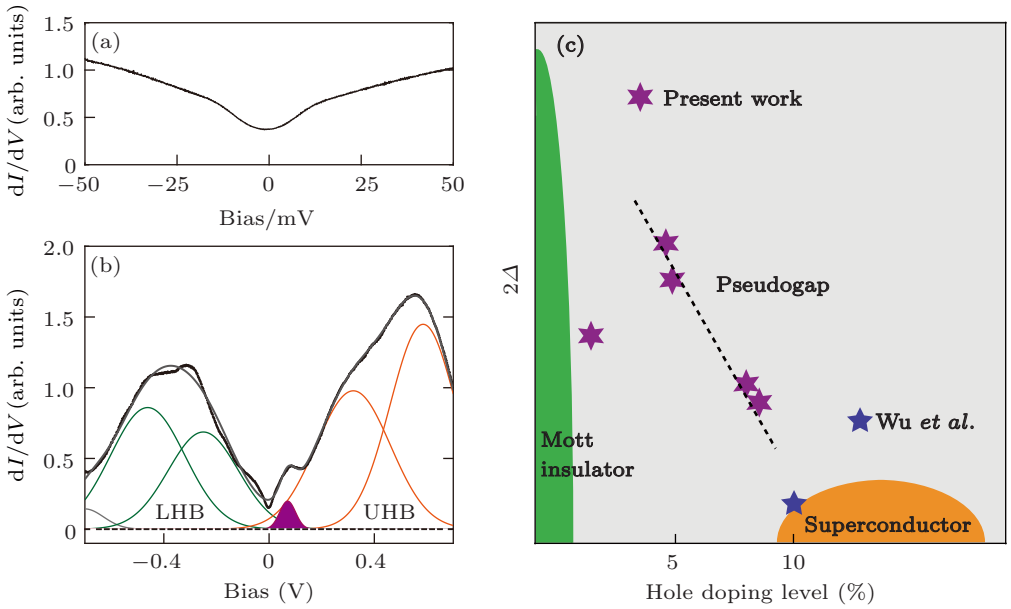


Fig. 4. (a), (b) Spatially averaged $\mathrm{d}I/\mathrm{d}V$ spectra on the $\sqrt{3}$-Sn grown on Si(111) with a resistivity of 0.01 Ω·cm, measured in the small and large energy-ranges, respectively. The large-energy-scale spectrum in (b) is fitted by multiple Gaussian peaks to obtain the doping level. Setpoint: (a) $V = 50$ mV, $I = 100$ pA; (b) $V = 1.0$ V, $I = 100$ pA. (c) Schematic electronic phase diagram of the modulation-doped $\sqrt{3}$-Sn by the underlying Si(111) substrates. The doping-dependent PG data are acquired on various $\sqrt{3}$-Sn domains in three samples, while the superconductivity one is adapted from Ref. [27].

4. Conclusion

We have spectroscopically observed an unusual PG and established the electronic phase diagram in a modulation-doped Mott insulator $\sqrt{3}$-Sn on the Si(111) substrates. The PG, electronic phase diagram, and chemical doping scheme are found to be analogous to those of the high-T_c cuprate superconductors. Further chemical doping control and experimental investigation of $\sqrt{3}$-Sn might find the microscopic mechanism of PG and superconductivity in this doped Mott insulator, by implications in cuprates.

Acknowledgments

Project supported by the National Natural Science Foundation of China (Grant Nos. 62074092 and 11604366) and the National Key R&D Program of China (Grant No. 2018YFA0305603).

References

[1] Mott N F 1961 *Philos. Mag.* **6** 287
[2] Mott N F 1982 *Proc. R. Soc. London Ser. A* **382** 1
[3] Belitz D and Kirkpatrick T R 1994 *Rev. Mod. Phys.* **66** 261
[4] Lee P A, Nagaosa N and Wen X G 2006 *Rev. Mod. Phys.* **78** 17
[5] Timusk T and Statt B 1999 *Rep. Prog. Phys.* **62** 61
[6] Fischer Ø, Kugler M, Maggio-Aprile I, Berthod C and Renner C 2007 *Rev. Mod. Phys.* **79** 353
[7] Damascelli A, Hussain Z and Shen Z X 2003 *Rev. Mod. Phys.* **75** 473
[8] Renner C, Revaz B, Genoud J Y, Kadowaki K and Fischer Ø 1998 *Phys. Rev. Lett.* **80** 149
[9] Chen Q J, Stajic J, Tan S and Levin K 2005 *Phys. Rep.* **412** 1
[10] Geshkenbein V B, Ioffe L B and Larkin A I 1997 *Phys. Rev. B* **55** 3173
[11] Loret B, Auvray N, Gallais Y, Cazayous M, Forget A, Colson D, Julien M H, Paul I, Civelli M and Sacuto A 2019 *Nat. Phys.* **15** 771
[12] Caprara S, Di Castro C, Seibold G and Grilli M 2017 *Phys. Rev. B* **95** 224511
[13] Kampf A P and Schrieffer J R 1990 *Phys. Rev. B* **42** 7967
[14] Zhang T, Cheng Peng, Li W J, Sun Y J, Wang G, Zhu X G, He K, Wang L L, Ma X C, Chen X, Wang Y Y, Liu Y, Lin H Q, Jia J F and Xue Q K 2010 *Nat. Phys.* **6** 104
[15] Uchihashi T, Mishra P, Aono M and Nakayama T 2011 *Phys. Rev. Lett.* **107** 207001
[16] Nakamura T, Kim H, Ichinokura S, Takayama A, Zotov A V, Saranin A A, Hasegawa Y and Hasegawa S 2018 *Phys. Rev. B* **98** 134505
[17] Özer M M, Thompson J R and Weitering H H 2006 *Nat. Phys.* **2** 173
[18] Matetskiy A V, Denisov N V, Hsing C R, Wei C M, Zotov A V and Saranin A A 2019 *J. Phys. Condens. Mat.* **31** 115402
[19] Carpinelli J M, Weitering H H, Plummer E W and Stumpf R 1996 *Nature* **381** 398
[20] Zhou Y H, Zhang P C, Fang Y M, Wu S Q and Zhu Z Z 2017 *Mater. Chem. Phys.* **199** 225
[21] Carpinelli J M, Weitering H H, Bartkowiak M, Stumpf R and Plummer E W 1997 *Phys. Rev. Lett.* **79** 2859
[22] Morikawa H, Matsuda I and Hasegawa S 2002 *Phys. Rev. Lett.* **65** 201308(R)
[23] Ottaviano L, Crivellari M, Lozzi L and Santucci S 2000 *Surf. Sci.* **445** L41
[24] Profeta G and Tosatti E 2007 *Phys. Rev. Lett.* **98** 086401
[25] Modesti S, Petaccia L, Ceballos G, Vobornik I, Panaccione G, Rossi G, Ottaviano L, Larciprete R, Lizzit S and Goldoni A 2007 *Phys. Rev. Lett.* **98** 126401
[26] Odobescu A B, Maizlakh A A, Fedotov N I and Zaitsev-Zotov S V 2017 *Phys. Rev. B* **95** 195151
[27] Wu X F, Ming F F, Smith T S, Liu G W, Ye F, Wang K Dong, Johnston S and Weitering H H 2020 *Phys. Rev. lett.* **125** 117001
[28] Hsu L and Walukiewicz W 1997 *Phys. Rev. B* **56** 1520
[29] Störmer H L and Tsang W T 1980 *Appl. Phys. Lett.* **36** 685
[30] People R, Bean J C, Lang D V, Sergent A M, Störmer H L, Wecht K W, Lynch R T and Baldwin K 1984 *Appl. Phys. Lett.* **45** 1231
[31] Zhong Y, Wang Y, Han S, Lv Y F, Wang W L, Zhang D, Ding H, Zhang Y M, Wang L L, He K, Zhong R D, Schneeloch J A, Gu G D, Song C L, Ma X C and Xue Q K 2016 *Sci. Bull.* **61** 1239
[32] Zhong Y, Fan J Q, Wang R F, Wang S Z, Zhang X F, Zhu Y Y, Dou Z Y, Yu X Q, Wang Y, Zhang D, Zhu J, Song C L, Ma X C and Xue Q K 2020 *Phys. Rev. Lett.* **125** 077002
[33] Ming F F, Smith T S, Johnston S, Snijders P C and Weitering H H 2018 *Phys. Rev. B* **97** 075403
[34] Ming F F, Johnston S, Mulugeta D, Smith T S, Vilmercati P, Lee G, Maier T A, Snijders P C and Weitering H H 2017 *Phys. Rev. Lett.* **119** 266802
[35] Wang R F, Guan J Q, Xiong Y L, Zhang X F, Fan J Q, Zhu J, Song C L, Ma X C and Xue Q K 2020 *Phys. Rev. B* **102** 100508(R)
[36] Hu C, Zhao J F, Gao Q, Yan H T, Rong H T, Huang J W, Liu J, Cai Y Q, Li C, Chen H, Zhao L, Liu G, Jin C Q, Xu Z Y, Xiang T and Zhou X J 2021 *Nat. Commun.* **12** 1
[37] Moukouri S, Allen S, Lemay F, Kyung B, Poulin D, Vilk Y M and Tremblay A M S 2000 *Phys. Rev. B* **61** 7887